



CHORUS

This is the accepted manuscript made available via CHORUS. The article has been published as:

Modeling amorphous thin films: Kinetically limited minimization

Paweł P. Zawadzki, John Perkins, and Stephan Lany

Phys. Rev. B **90**, 094203 — Published 16 September 2014

DOI: [10.1103/PhysRevB.90.094203](https://doi.org/10.1103/PhysRevB.90.094203)

Modeling amorphous thin films: Kinetically limited minimization

Pawel Zawadzki, John Perkins, and Stephan Lany

National Renewable Energy Laboratory, Golden, CO, USA

ABSTRACT

Atomic-scale models of amorphous structures are typically generated using simulated annealing (SA) quench from a melt simulation protocol. This approach resembles the preparation of bulk glasses, but it may not be suitable for modeling amorphous materials produced using low-energy and low-temperature physical vapor deposition (PVD), where a deposited atom induces only local relaxations and no equilibrated melt is formed. To account for such growth conditions, we developed the kinetically limited minimization (KLM) technique, in which an amorphous structure is constructed from a randomly initialized structure in a number of local perturbation-relaxation steps. We compare formation energies as well as short- and medium-range order of KLM- and SA-generated structures of a-In₂O₃, a-ZnO, and a-Si.

I. INTRODUCTION

Amorphous materials are becoming increasingly attractive as functional components in thin-film devices such as thin-film displays and solar cells [1]. Due to lack of grain boundaries, they have superior uniformity and smoothness, flexibility, and corrosion resistance [1,2]. Amorphous oxides with highly dispersive conduction bands—such as a-In₂O₃, a-SnO₂, or ternary oxides like a-InZnO—maintain high electron mobilities similar to those in crystalline transparent conductive oxides [3,4]. To prevent crystallization,

amorphous thin films are prepared at low temperatures, typically using sputtering deposition techniques [5,6]. However, computational models of amorphous structures, which are needed for electronic structure predictions, are almost exclusively constructed with a simulated annealing (SA) protocol starting from a high-temperature, equilibrated crystal melt [7–11]. Although such a procedure imitates the quench from the melt preparation of bulk glasses, its applicability to modeling low-temperature synthesized amorphous materials is unclear. Simulated annealing is necessarily a global optimization technique, where all atomic positions are simultaneously relaxed, and given a sufficiently slow quench rate, this optimization approach will lead to the ground-state structure. From the perspective of low-temperature deposition, one can approach the problem of structure optimization from a different limit, i.e., from an initial random atomic structure that evolves through a sequence of atomic movements. If the individual events are sufficiently separated in time and space, the correlated simultaneous movement of multiple atoms is suppressed, and the structure will generally approach a metastable configuration—with a certain amount of energy above the ground state—but will not relax into the crystalline ground-state. We here address this scenario by a kinetically limited minimization (KLM) that starts from a randomly initialized structure and minimizes the total energy through sequential local perturbation-relaxation events. Compared to the stochastic quench method [12], where amorphous structures are generated by a direct quench of a random structure to the nearest local minima, KLM removes compositional inhomogeneities and highly unstable local configurations that are present in randomly generated structures.

Physical vapor deposition of amorphous films, usually employing sputtering techniques, can produce thin films with different degrees of thermodynamic stability and

structural order, ranging from amorphous materials to crystalline phases. The two most important growth parameters that control the outcome of deposition processes are the growth temperature and the energetics of sputtered atoms that impinge on the surface [6,13–15]. Amorphous oxides are typically prepared at, or slightly above, room temperature [16,17], i.e., well below the melting point (for instance, $T_m(\text{In}_2\text{O}_3) = 2183$ K and $T_m(\text{ZnO}) = 2248$ K [18]). At such temperatures ($<0.2 T_m$ [K]), atomic diffusion is limited [6,13] and the impact of deposited atoms and sputter gas atoms becomes the most important source of energy available for structural relaxation. An important question in regard to the model for the computational structure generation is whether, at the relevant ion energies, (1) the so-called “thermal spike” [12,19,20] caused by impinging ions is sufficient to locally melt the crystal, or (2) the ion impact causes only the displacement of one or a few atoms.

We compare KLM and SA of a crystal melt with quench rates ranging from 64 to 2500 K/ps using prototypical ionic (In_2O_3 and ZnO) and covalent (Si) materials. In the KLM approach, the enthalpy approaches a value below the fast-quench SA, but above that of the slow quench. KLM provides short-range order that corresponds differently to quench-rate SA for different materials: fast quench for a- In_2O_3 and slow quench for a- ZnO and a-Si. This observation indicates that kinetic limitations play an important role in the development of the local structure. Because correlated relaxations are limited in KLM, the method predicts medium-range order similar to that of fast-quench SA.

II. COMPUTATIONAL DETAILS

A. Generation of amorphous structures

Amorphous In_2O_3 , ZnO , and Si structures were modeled in 160-atom periodic cells using SA molecular dynamics and KLM. The simulated annealing was performed in the canonical (NVT) ensemble with the Nosé–Hoover thermostat using the Verlet algorithm with 4 fs integration step. The following simulation protocol was used: First, the respective crystal as well as randomly generated structures were melted and equilibrated for 15 ps at 2500 K for the case of In_2O_3 , ZnO and at 3000 K for the case of Si . The temperature was then lowered to 500 K at rates ranging from 64 to 2500 K/ps. In the last step, volumes and atomic positions of the final structures were relaxed. The kinetically limited minimization, which, in essence, relaxes a structure by a number of sequential local perturbation-relaxation events, is described below. As a starting point for this algorithm, we used five random structures with an imposed minimum inter-atomic distance equal to the respective bond distances in crystalline material minus 0.3 Å. After 300 relaxation-perturbation steps, the algorithm was terminated and, as in case of SA, volume and atomic positions relaxed.

B. Thermal spike simulations

In addition, we performed molecular dynamics simulation of kinetic energy dissipation in the In_2O_3 crystal. First, In_2O_3 was equilibrated at 300 K in a canonical ensemble. Then, the velocity of the In or O atom was increased in a random direction such that the atom has the kinetic energy equal to 1, 5, or 30 eV. The micro-canonical ensemble was then simulated for 6 ps using the maximum time step of 0.86, 0.37 and 0.15 fs for systems with 1-, 5-, and 30-eV accelerated atom, respectively. Forces and energies were obtained from density functional theory (DFT) calculations with the PBE

exchange correlation functional [21] within the PAW formalism as implemented in the VASP code [22]. For the final relaxation of amorphous structures, a $2 \times 2 \times 2$ Monkhorst Pack mesh was used. For the computationally expensive SA molecular dynamics and KLM, we used a single k-point sampling.

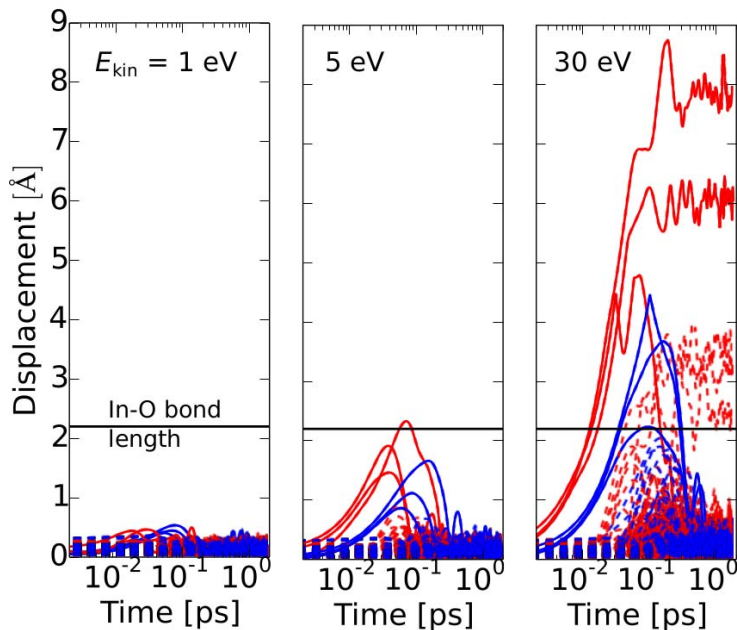


FIG. 1: (Color online) Atomic displacements induced by 1-, 5- and 30-eV accelerated In and O atoms in $c\text{-In}_2\text{O}_3$ as a function of time. Each plot shows the results of six simulations (three for In and three for O atom). Full lines: the accelerated atoms, dashed lines: the remaining atoms; blue: In, red: O.

III. THERMAL SPIKE SIMULATIONS

Application of quench from melt methods to modeling amorphous thin films is often justified by the fact that energetic impact during deposition creates a local melt (a thermal spike) in which simultaneous and long-range atomic rearrangements are possible [19]. In the following, we estimate the degree of relaxation induced by impact

of atoms with kinetic energy of up to 30 eV. Such energies have been linked to low-stress growth conditions of amorphous materials [13,15,23]. Figure 1 shows the atomic displacement induced by accelerated In and O atoms with a kinetic energy of 1, 5, and 30 eV in crystalline In_2O_3 equilibrated at 300 K (thermal energy of 0.04 eV/atom). The red and blue full lines show the evolution of the amplitude of the accelerated O and In atoms, respectively. The indium and oxygen atoms with kinetic energy of 1 eV displace by up to 0.7 Å beyond their respective equilibrium positions, which is much less than the nearest-neighbor distance of 2.2 Å in In_2O_3 . At lower energies, the deposited atoms are likely to condensate without penetrating the surface, and the impact energy produces hardly any relaxation events below the surface. For kinetic energy of 5 eV, the maximal amplitude of both In and O atoms is ~ 1.5 Å, and for channeling directions it may exceed the nearest-neighbor distance and be sufficient for the deposited atom to penetrate into subsurface layers. Thus, at energies of several eV, the bulk structure beneath the growing surface starts to relax, lowering the energy with respect to the structure determined by the surface condensation on a budget of less than one relaxation event on average per deposited atom. At 1 and 5 eV, only the accelerated atom itself shows a displacement amplitude above 1 Å, so the induced relaxation is local and limited to, at most, the nearest neighbors of the accelerated atom. After the dissipation of the energy due to the acceleration, all atoms return to their initial position. In contrast, a 30-eV impact induces displacements beyond the In-O distance, not only of the accelerated atom but also of the neighboring atoms. Thus, at this energy, the impinging atom may penetrate into subsurface layers and induce relaxations involving further coordination shells. Similarly to the 1- and 5-eV impacts, the 30-eV impact also equilibrates in less than 1 ps, i.e., the same order of

magnitude as the phonon frequency. Such fast dissipation times do not allow for full equilibration of the molten state, which typically requires 1–2 orders of magnitude longer timescales [7,24]. (Note that the heat-diffusion laws based on the macroscopic thermal conductivity overestimate the lifetime because the size of the thermal spike is much smaller than the phonon mean free path.) Instead, the perturbation of the ion impact causes a few individual relaxation events at the most, rather than a local melting. These results for In_2O_3 are in line with the general models for stress generation in thin-film deposition [13,23,25,26], suggesting surface condensation and void formation at low impact energies of up to several eV, the coalescence of such voids and limited relaxation at moderate energies, and, at high energies in the keV range, the occurrence of a thermal spike with sufficiently high energy and long lifetime to cause a local melting and stress relief.

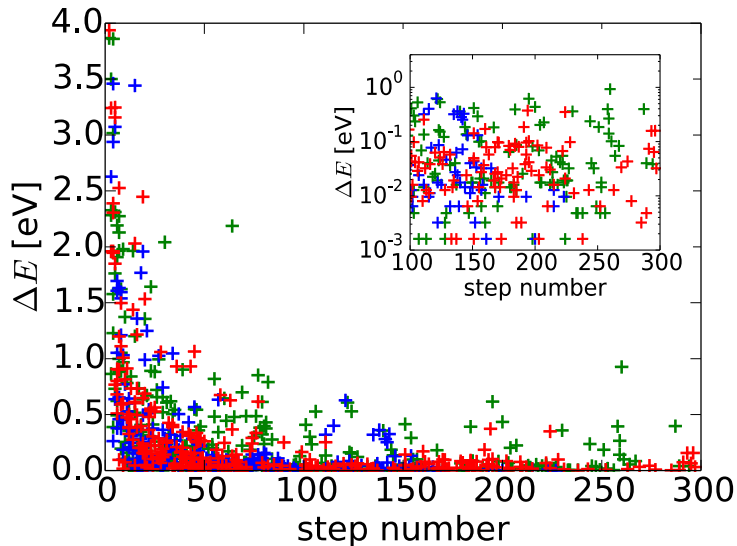


Fig. 2 (Color online) The change in energy of accepted moves during kinetically limited

minimization as a function of a step number. Red: a-In₂O₃; blue: a-ZnO; and green: a-Si (five runs for each material).

IV. KINETICALLY LIMITED MINIMIZATION

In view of the preceding discussion, we formulate a method for modeling amorphous structures by a sequence of individual local perturbation-relaxation events, which should be more appropriate than a melt-quench protocol for physical vapor deposition techniques with low to moderate (< 100 eV) ion energies. The proposed algorithm consists of four steps. For a given initial structure, we first find structural void centers by following the gradient of the distance field $D(\vec{r})$ from a randomly selected point (step 1). A void center is defined as a local maximum of a distance field $D(\vec{r})$ — a scalar quantity that measures at a given point \vec{r} the distance to the nearest atom: $D(\vec{r}) = \min_i |\vec{r} - \vec{r}_i|$, where \vec{r}_i are atomic positions. Once a void center is selected, we displace the nearest atom into the void (step 2). Such a move constitutes the minimal local perturbation that allows for diffusive motion necessary to remove compositional gradients that are present in randomly generated structures. After the perturbation step, we relax the structure to the nearest local minimum (step 3). If such a perturbation-relaxation event lowers the energy, we accept the move and update the structure; otherwise, we reject it (step 4). In essence, this is a basin-hopping algorithm with the Monte Carlo step being a local structural perturbation and with the Metropolis acceptance criterion at 0 K. Figure 2 shows the change in energy (ΔE) of accepted moves during KLM runs starting from five different random structures of a-In₂O₃, a-ZnO, and a-Si. Initially, structures relax in steps involving $\Delta E > 0.5$ eV energy changes. This indicates that random structures, even if

relaxed to the nearest local minima as in stochastic quench method [12], contain a large number of highly unstable local configurations. Such high-energy configurations are largely removed after ~ 150 steps.

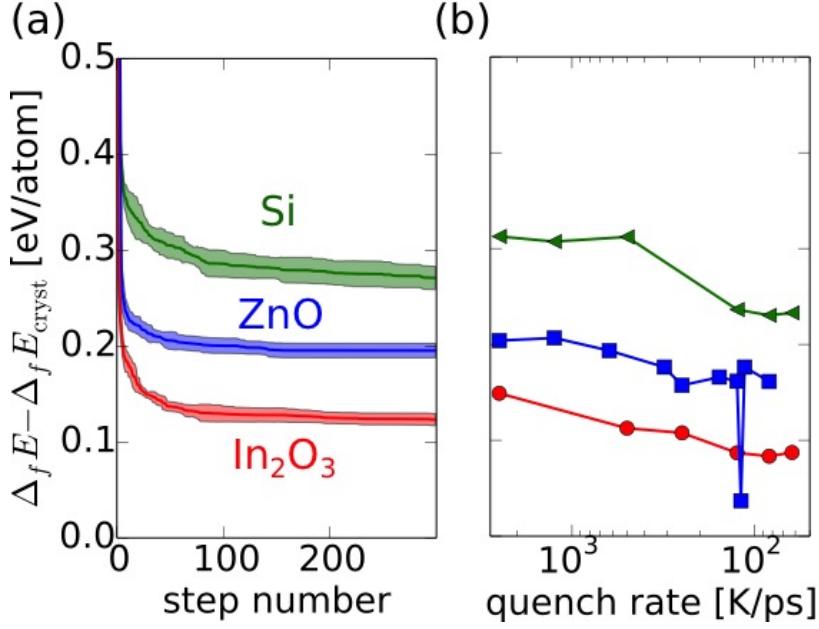


FIG. 3: (Color online) Formation energies of amorphous structures relative to formation energy of the respective ground-state crystal structure for a-Si (green), a-ZnO (blue), and a-In₂O₃ (red), as a function of the (a) step number of KLM and (b) quench rate of SA. The green, blue and red bands in subfigure (b) denote two standard deviations calculated from four different initial random structures.

V. ENTHALPY

Figure 3 shows the formation energies of the amorphous structures with respect to crystal phase of amorphous structure, comparing the KLM with the SA for different quench rates ranging from 64 to 2500 K/ps. The KLM energies lie in between the SA energies for fast and slow quenches, indicating that SA quenches at rates accessible with

ab initio molecular dynamics (MD) can lead to enthalpies significantly below those of the kinetically limited structure evolution. At sufficiently slow quench rates, the SA would lead to complete crystallization ($\Delta E = 0$), and indeed, we observed crystallization and a very low ΔE for the SA of ZnO at the rate 110 K/ps. The crystallization is, of course, facilitated by the periodic boundary conditions of the simulation cell. But this observation also may reflect the fact that ZnO crystallizes relatively easily and is difficult to obtain in the amorphous structure, even at low (room) temperature deposition [27]. Unlike the SA enthalpy, which depends strongly on the quench rate, the KLM enthalpy approaches a unique limit, i.e., the kinetically limited structure evolution. It is worth noting, however, that amorphous structures are generally in a much more dynamic state than crystalline structures: In a perfect crystalline structure, atomic rearrangement creates lattice defects that usually have sizable formation enthalpies. In the amorphous structure, there is a much larger number of configurations close in energy ($\Delta E < 0.1$ eV, as seen in Fig. 2), enabling continuous lattice reconfigurations. This aspect of amorphous semiconductors could be exploited to design materials with the ability to self-heal when detrimental defects are created, e.g., by processing during device fabrication. Given the same degree of structural relaxation— i.e., step number in the case of KLM, or quench rate in the case of SA—both methods provide qualitatively the same differences between formation energies. This observation allows us to order a-Si, a-ZnO, and a-In₂O₃ in terms of their thermodynamic driving force for crystallization: a-In₂O₃ exhibits the lowest and a-Si the highest value.

VI. SHORT- AND MEDIUM-RANGE ORDER

Figure 4 shows the distribution of the first shell coordination numbers (CNs) in

crystal (c), liquid (l), and amorphous (a) In_2O_3 , ZnO , and Si calculated with cutoff distances of 2.9, 2.7 and 2.9 Å, respectively. In all three cases, the CN distribution in liquid broadens as compared to crystal phase. Both fast- and slow-quench SA bring down the CN closer to crystal values. The difference between the liquid and amorphous phase is particularly large in the case of ZnO and Si liquid, where the CN distribution is shifted toward higher coordination numbers [27]. The quench of l- In_2O_3 , on the other hand, leads to relatively small changes in the CN distribution, and a- In_2O_3 retains a significant number of 5-fold-coordinated In and 3-fold-coordinated O atoms (in agreement with previous MD simulations [9]). The concentration of 5-fold coordinated In atoms in a- In_2O_3 is 16, 30 and 34 % and 3-fold coordinated O atoms is 11, 17 and 23 % for slow quench SA, fast quench SA and KLM, respectively. KLM also finds 4-fold coordinated In atoms, though at very small concentration of 1%. This deviation from the crystalline coordination may be due to kinetic limitations (structural frustrations) and/or lower thermodynamic driving force to crystallization of a- In_2O_3 mentioned in the previous paragraph. KLM leads to qualitatively the same CN distribution as SA but quantitative differences are evident. For a- ZnO and a- Si , the CN distribution of KLM generated structures corresponds to slow quench, whereas for a- In_2O_3 , it corresponds to fast-quench SA. Thus, correlated atomic relaxations in a- In_2O_3 lead to stronger local ordering. This observation indicates that the development of the short-range order in this material is more kinetically limited than in a- ZnO or a- Si .

To characterize the medium-range order we plot partial pair distribution functions in Fig. 5. Overall, both KLM and SA show that medium-range order in a- In_2O_3 and a- ZnO is far stronger compared to covalently bonded a- Si , where ordering beyond 6 Å is

negligible. This is likely because of the importance of long-range electrostatic interactions in ionic compounds. Particularly strong medium-range order is seen in the In-In pair distribution, because In has a +3 formal charge and low polarizability (ionic radius of 0.8 Å), leading to strong electrostatic In-In repulsion. In KLM, the formation of medium-range order is limited, and as a result, KLM predicts a similar degree of medium-range order as SA with fast-quench rate.

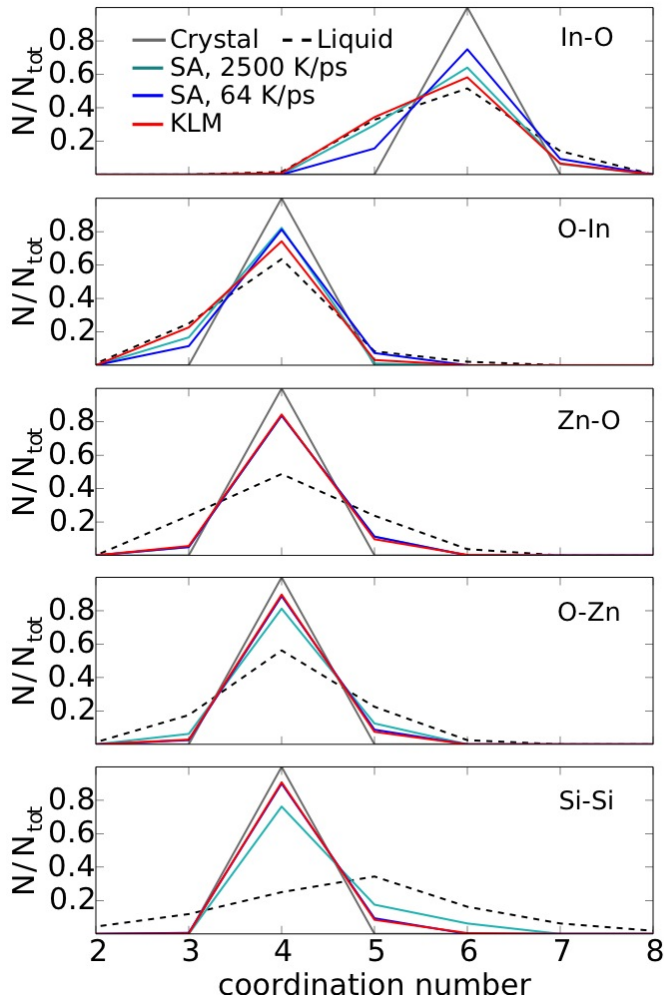


FIG. 4: (Color online) Distribution of coordination numbers in crystal (solid black line), liquid (dashed black line), and amorphous In_2O_3 , ZnO , and Si (solid lines: blue and cyan for SA with quench rate 64 and 2500 K/ps, respectively, and red for KLM).

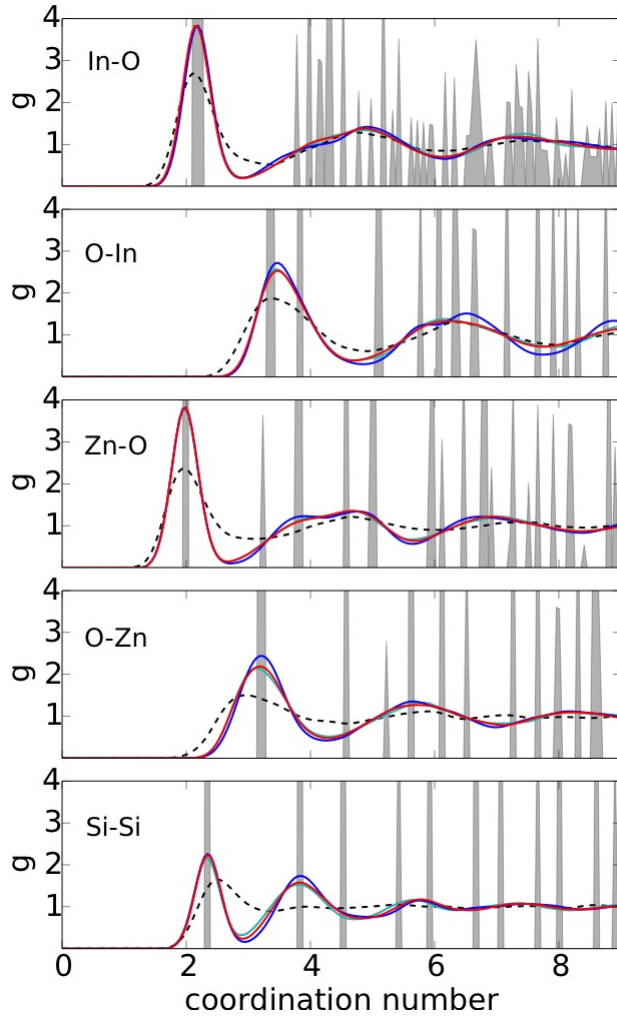


FIG. 5: (Color online) Partial pair distribution functions in crystal (solid black line), liquid (dashed black line), and amorphous In_2O_3 , ZnO , and Si (solid lines: blue and cyan for SA with quench rate 64 and 2500 K/ps, respectively, and red for KLM).

VII. CONCLUSIONS

In conclusion, we addressed the problem of generating structural models for amorphous thin-film semiconductors that are formed by low-temperature deposition

considerably below the melting temperature. For typical ion energies, e.g., in sputtering deposition, the thermal spike dissipates too fast to create a local melt. Therefore, we formulated an alternative approach to the conventional melt-quench simulated annealing (SA) protocol. Starting from initial random atomic positions, the structure is updated by kinetically limited minimization (KLM), i.e., by sequential local perturbation-relaxation events. Unlike the SA approach, where the enthalpy and degree of crystallization depend strongly on the quench rate, the KLM approaches a steady state whose energy lies slightly below that of a fast-quenched melt. Depending on the particular material, short-range order of KLM-generated structures corresponds to different quench rates in SA. This indicates that kinetic limitations play an important role in the development of local structure. Because relaxations in KLM are necessarily local, the method produces structures with the medium-range order similar to the one from fast-quench SA.

ACKNOWLEDGMENTS

This work was supported through the SunShot Initiative funded by the U.S. Department of Energy, Office of Energy Efficiency and Renewable Energy, Office of Solar Energy Technology under Award Number DE-AC36-08GO28308 to NREL. The computing resources of the High Performance Computing center at NREL are gratefully acknowledged.

- [1] T. Kamiya and H. Hosono, *NPG Asia Mater.* **2**, 15 (2010).
- [2] C.-C. Shih, S.-J. Lin, K.-H. Chung, Y.-L. Chen, and Y.-Y. Su, *J. Biomed. Mater. Res.* **52**, 323 (2000).

- [3] K. Nomura, H. Ohta, A. Takagi, T. Kamiya, M. Hirano, and H. Hosono, *Nature* **432**, 488 (2004).
- [4] H. S. Kim, M.-G. Kim, Y.-G. Ha, M. G. Kanatzidis, T. J. Marks, and A. Facchetti, *J. Am. Chem. Soc.* **131**, 10826 (2009).
- [5] G. Bräuer, B. Szyszka, M. Vergöhl, and R. Bandorf, *Vacuum* **84**, 1354 (2010).
- [6] A. Anders, *Thin Solid Films* **518**, 4087 (2010).
- [7] J. Rosen and O. Warschkow, *Phys. Rev. B* **80**, 115215 (2009).
- [8] A. Aliano, A. Catellani, and G. Cicero, *Appl. Phys. Lett.* **99**, 211913 (2011).
- [9] J. Rosen, O. Warschkow, D. R. McKenzie, and M. M. M. Bilek, *J. Chem. Phys.* **126**, 204709 (2007).
- [10] J. Houska, J. Capek, J. Vlcek, M. M. M. Bilek, and D. R. McKenzie, *J. Vac. Sci. Technol. A, Vacuum, Surfaces, Film* **25**, 1411 (2007).
- [11] J. Houska and S. Kos, *J. Phys. Condens. Matter* **23**, 25502 (2011).
- [12] C. Arhammar, A. Pietzsch, N. Bock, E. Holmström, C. M. Araujo, J. Gråsjö, S. Zhao, S. Green, T. Peery, F. Hennies, S. Amerioun, A. Föhlisch, J. Schlappa, T. Schmitt, V. N. Strocov, G. A. Niklasson, D. C. Wallace, J.-E. Rubensson, B. Johansson, and R. Ahuja, *Proc. Natl. Acad. Sci.* **108**, 6355 (2011).
- [13] O. R. Monteiro, *Annu. Rev. Mater. Res.* **31**, 111 (2001).
- [14] H. Hensel and H. Urbassek, *Phys. Rev. B* **58**, 2050 (1998).
- [15] J. Vlcek, S. Potocký, J. Čížek, J. Houska, M. Kormunda, P. Zeman, V. Perina, J. Zemek, Y. Setsuhara, and S. Konuma, *J. Vac. Sci. Technol. A Vacuum, Surfaces, Film.* **23**, 1513 (2005).
- [16] H. Nakazawa, Y. Ito, E. Matsumoto, K. Adachi, N. Aoki, and Y. Ochiai, *J. Appl. Phys.* **100**, 93706 (2006).
- [17] J. M. Khoshman and M. E. Kordesch, *Thin Solid Films* **515**, 7393 (2007).
- [18] D. R. Lide, *CRC Handbook of Chemistry and Physics* (CRC press, 2003).
- [19] N. A. Marks, *Phys. Rev. B* **56**, 2441 (1997).
- [20] A. Meftah, F. Brisard, J. M. Costantini, E. Dooryhee, M. Hage-Ali, M. Hervieu, J. P. Stoquert, F. Studer, and M. Toulemonde, *Phys. Rev. B* **49**, 12457 (1994).
- [21] J. P. Perdew, K. Burke, and M. Ernzerhof, *Phys. Rev. Lett.* **78**, 1396 (1997).

- [22] G. Kresse and D. Joubert, *Phys. Rev. B* **59**, 1758 (1999).
- [23] M. M. M. Bilek and D. R. McKenzie, *Surf. Coatings Technol.* **200**, 4345 (2006).
- [24] K. Harafuji, T. Tsuchiya, and K. Kawamura, *J. Appl. Phys.* **96**, 2501 (2004).
- [25] A. Lefèvre, L. Lewis, L. Martinu, and M. Wertheimer, *Phys. Rev. B* **64**, 115429 (2001).
- [26] M. Koster and H. M. Urbassek, *Surf. Sci.* **496**, 196 (2002).
- [27] K. Ellmer, A. Klein, and B. Rech, editors, *Transparent Conductive Zinc Oxide* (Springer-Verlag, 2008), p. 9.
- [28] I. Stich, R. Car, and M. Parrinello, *Phys. Rev. B* **44**, 11092 (1991).

Electronic address: slany@nrel.gov